

## Ab initio intermolecular potential energy surface and thermophysical properties of nitrous oxide

Johann-Philipp Crusius, Robert Hellmann, Egon Hassel, and Eckard Bich

Citation: *The Journal of Chemical Physics* **142**, 244307 (2015); doi: 10.1063/1.4922830

View online: <http://dx.doi.org/10.1063/1.4922830>

View Table of Contents: <http://scitation.aip.org/content/aip/journal/jcp/142/24?ver=pdfcov>

Published by the **AIP Publishing**

---

### Articles you may be interested in

[Ground state analytical ab initio intermolecular potential for the Cl<sub>2</sub>-water system](#)

*J. Chem. Phys.* **142**, 144310 (2015); 10.1063/1.4917028

[Intermolecular potential energy surface and thermophysical properties of ethylene oxide](#)

*J. Chem. Phys.* **141**, 164322 (2014); 10.1063/1.4899074

[Theoretical studies of the N<sub>2</sub>O van der Waals dimer: Ab initio potential energy surface, intermolecular vibrations and rotational transition frequencies](#)

*J. Chem. Phys.* **134**, 054311 (2011); 10.1063/1.3523984

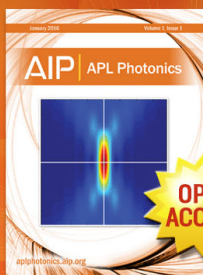
[Nitrous oxide dimer: A new potential energy surface and rovibrational spectrum of the nonpolar isomer](#)

*J. Chem. Phys.* **133**, 134304 (2010); 10.1063/1.3494542

[Ab initio potential-energy surface for the He \( 1 S\)+ NO \(X 2 Π\) interaction and bound rovibrational states](#)

*J. Chem. Phys.* **112**, 2195 (2000); 10.1063/1.480785

---



Launching in 2016!

The future of applied photonics research is here

**OPEN  
ACCESS**

**AIP** | APL  
Photonics

# Ab initio intermolecular potential energy surface and thermophysical properties of nitrous oxide

Johann-Philipp Crusius,<sup>1,a)</sup> Robert Hellmann,<sup>2,b)</sup> Egon Hassel,<sup>1</sup> and Eckard Bich<sup>2</sup>

<sup>1</sup>Lehrstuhl für Technische Thermodynamik, Universität Rostock, 18059 Rostock, Germany

<sup>2</sup>Institut für Chemie, Universität Rostock, 18059 Rostock, Germany

(Received 5 April 2015; accepted 11 June 2015; published online 25 June 2015)

We present an analytical intermolecular potential energy surface (PES) for two rigid nitrous oxide ( $N_2O$ ) molecules derived from high-level quantum-chemical *ab initio* calculations. Interaction energies for 2018  $N_2O$ - $N_2O$  configurations were computed utilizing the counterpoise-corrected supermolecular approach at the CCSD(T) level of theory using basis sets up to aug-cc-pVQZ supplemented with bond functions. A site-site potential function with seven sites per  $N_2O$  molecule was fitted to the pair interaction energies. We validated our PES by computing the second virial coefficient as well as shear viscosity and thermal conductivity in the dilute-gas limit. The values of these properties are substantiated by the best experimental data. © 2015 AIP Publishing LLC. [<http://dx.doi.org/10.1063/1.4922830>]

## I. INTRODUCTION

Precise values for thermophysical properties of fluids are of great interest for use in industrial applications and natural sciences. In our previous work, see, for instance, Refs. 1–5 and references therein, we have demonstrated that accurate thermophysical property values of dilute gases can be determined using high-quality intermolecular pair potentials. Employing quantum-chemical *ab initio* methods, potential energy surfaces (PESs) of small molecule pairs can be obtained with high accuracy with today's computing power. From these pair potentials, one can calculate, for example, second virial coefficients from statistical thermodynamics or transport and relaxation properties in the dilute-gas limit using the kinetic theory of molecular gases.<sup>3,6,7</sup> Determining values of thermophysical properties from theory is of particular interest when experimental conditions are difficult or dangerous to handle.

Nitrous oxide ( $N_2O$ ) is an important industrial fluid with a wide range of applications. It is used, for example, as an anesthetic in medicine, as a propellant in food industry, and as a performance increasing oxidant in rockets and piston engines.

In the past, several studies have dealt with identifying the minimum structures of the  $N_2O$  dimer through spectroscopic measurements<sup>8,9</sup> or by means of quantum-chemical calculations.<sup>10,11</sup> Scans of the entire PES have only been undertaken in recent years.<sup>12,13</sup> In 2010, Dawes *et al.*<sup>12</sup> have calculated interaction energies for 1757 configurations at the CCSD(T)-F12b<sup>14,15</sup>/VTZ-F12<sup>16</sup> level. They used interpolating moving least-squares (IMLS) fitting to identify the stationary points on the PES and to calculate rovibrational properties. In 2011, Zheng *et al.*<sup>13</sup> have calculated interaction energies for about 10 000 points on the PES using the CCSD(T)<sup>15</sup> method with the aug-cc-pVTZ<sup>17</sup> basis set supplemented by bond functions also for studying the minimum structures

and rovibrational properties. They evaluated their PES using Lagrange interpolation. Until today, there appears to exist no closed analytical formulation of a high-quality PES for  $N_2O$ .

In the present paper, we applied the counterpoise-corrected supermolecular approach<sup>18</sup> to determine interaction energies at the CCSD(T) level of theory for more than 2000 dimer configurations using basis sets of triple-zeta and quadruple-zeta quality supplemented with additional bond functions. The calculated interaction energies were extrapolated to the complete basis set (CBS) limit. An analytical seven-center site-site potential function with isotropic site-site interactions was fitted to the extrapolated interaction energies. We validated our proposed PES by calculating the second virial coefficient using statistical thermodynamics as well as shear viscosity and thermal conductivity for the dilute gas employing the classical trajectory approach in conjunction with the kinetic theory of gases for rigid linear molecules.<sup>4,6,7,19</sup>

In Sec. II, we describe the development of the analytical potential function. In Sec. III, we present the theory and the results for the second virial coefficient and do the same for the transport properties in Sec. IV. Summary and conclusions are given in Sec. V.

## II. INTERMOLECULAR POTENTIAL

### A. Monomer geometry

Considering all degrees of freedom of the  $N_2O$  dimer, the intermolecular potential is a 12-dimensional hypersurface. Past experience with small molecules, see, for example, Refs. 4 and 20–23, justifies treating the  $N_2O$  monomers as rigid rotors in their zero-point vibrationally averaged geometry, which yields a four-dimensional, but still highly accurate PES. The zero-point vibrationally averaged geometry of  $N_2O$  that was used in all quantum-chemical *ab initio* calculations features an N–N bond length of 1.127 80 Å and an N–O bond length of 1.188 56 Å. This geometry was obtained as follows.

<sup>a)</sup>Electronic mail: johann-philipp.crusius@uni-rostock.de.

<sup>b)</sup>Electronic mail: robert.hellmann@uni-rostock.de.

First, the structure of the N<sub>2</sub>O monomer was optimized at the all-electron CCSD(T)/cc-pwCVQZ<sup>24</sup> level, yielding an equilibrium N–N bond length of 1.126 66 Å and an N–O bond length of 1.184 74 Å. Then, a cubic force field calculation was performed at the same level of theory, giving a zero-point vibrationally averaged geometry with  $r_{\text{NN}} = 1.128\ 85$  Å and  $r_{\text{NO}} = 1.188\ 90$  Å. Finally, the differences in the bond length from these two calculations were added to the equilibrium bond lengths at the all-electron CCSD(T)/cc-pCV6Z level of theory with  $r_{\text{NN}} = 1.125\ 61$  Å and  $r_{\text{NO}} = 1.184\ 40$  Å. Such an approach usually yields reliable geometries, which are consistent with data obtained by spectroscopic methods, as we have observed in our previous work, see, for example, Refs. 4 and 5. Our values are also in good agreement with the calculated values of Chang *et al.*<sup>25</sup>

## B. *Ab initio* calculation of interaction energies

The geometry of a pair of rigid N<sub>2</sub>O molecules can be expressed as a function of the four variables  $R$ ,  $\theta_1$ ,  $\theta_2$ , and  $\phi$ , where  $R$  is the distance between the centers of mass of the two monomers,  $\theta_1$  and  $\theta_2$  are the angles between the  $R$  axis and the respective bond vectors of molecules 1 and 2, and  $\phi$  marks the dihedral angle. The bond vector points from the nitrogen atoms towards the oxygen atom. Due to symmetry, it is sufficient to consider an angular range of  $0^\circ \leq (\theta_1, \theta_2, \phi) \leq 180^\circ$ . One hundred symmetry unique angular configurations were generated by varying the  $\theta$  angles in steps of  $30^\circ$ , while  $\phi$  was varied in steps of  $45^\circ$  for  $(\theta_1 \vee \theta_2) \in \{0^\circ, 30^\circ, 150^\circ, 180^\circ\}$  and in steps of  $30^\circ$  for  $(\theta_1 \wedge \theta_2) \in \{60^\circ, 90^\circ, 120^\circ\}$ . Twenty two separations of  $R$  in the range of 2.0 Å–10.0 Å were considered. Configurations in which two atoms were too close to each other, or for which linear dependencies in the basis sets resulted in the failure of the quantum-mechanical calculations, were discarded. This resulted in 2016 useable configurations. Two further configurations were added, which represent the minima identified in a preliminary fit of the PES based on the initial 2016 configurations, yielding a total of 2018 configurations.

Using the supermolecular approach including the full counterpoise correction at the frozen-core CCSD(T) level of theory, we have determined the pair interaction energies  $V(R, \theta_1, \theta_2, \phi)$  for all 2018 configurations utilizing the aug-cc-pVXZ basis sets<sup>17</sup> for  $X = 3(\text{T})$  and  $X = 4(\text{Q})$ . Both basis sets were supplemented by a small  $3s3p2d1f$  set of bond functions located midway along the  $R$ -axis, the exponents being 0.1, 0.3, and 0.9 for  $s$  and  $p$ , 0.25 and 0.75 for  $d$ , and 0.45 for  $f$ .

The correlation parts of the calculated interaction energies,  $V_{\text{CCSD(T) corr}}$ , were extrapolated to the CBS limit using the well-tried two-point extrapolation scheme of Halkier *et al.*,<sup>26</sup>

$$V_{\text{CCSD(T) corr}}(X) = V_{\text{CCSD(T) corr}}^{\text{CBS}} + \alpha X^{-3}. \quad (1)$$

Since the Hartree-Fock (HF) contributions converge much faster to the CBS limit than the correlation contributions, the HF values from the aug-cc-pVQZ calculations were taken as a good HF-CBS approximation.

We then obtained the final interaction energies by adding the extrapolated CCSD(T) correlation energies to the HF/

aug-cc-pVQZ energies,

$$V_{\text{final}} = V_{\text{SCF}}^{\text{QZ}} + V_{\text{CCSD(T) corr}}^{\text{CBS}} \quad (2)$$

For some strongly repulsive configurations (usually  $V \gg 5000$  K), the CCSD(T)/aug-cc-pVQZ calculations did not converge. In these cases, we used the CCSD(T)/aug-cc-pVTZ values as the final interaction energies to allow for a stable analytical fit. This approach is justified by the fact that the strongly repulsive regions of the PES play a rather insignificant role in the determination of thermophysical properties. This has been accounted for in the weighting for the strongly repulsive values during the fit. The detailed results of our *ab initio* calculations for all 2018 configurations can be found in the electronic supplementary material.<sup>27</sup>

All quantum-chemical calculations reported in this work have been carried out using the cfour program.<sup>28</sup>

## C. Analytical potential function

We fitted a site-site potential function with seven sites per molecule to the calculated interaction energies. This results in 28 different types of site-site combinations. The site positions were initially chosen intuitively within the N<sub>2</sub>O monomer and subsequently treated as free parameters during the fit. The functional form describing each site-site interaction is given by

$$V_{ij}(R_{ij}) = A_{ij} \exp(-\alpha_{ij} R_{ij}) - f_6(R_{ij}, b_{ij}) \frac{C_{6ij}}{R_{ij}^6} - f_8(R_{ij}, b_{ij}) \frac{C_{8ij}}{R_{ij}^8} + \frac{q_i q_j}{R_{ij}}, \quad (3)$$

where  $R_{ij}$  is the distance between site  $i$  in molecule 1 and site  $j$  in molecule 2, and  $f_6$  and  $f_8$  are damping functions as given by Tang and Toennies,<sup>29</sup>

$$f_n(R_{ij}, b_{ij}) = 1 - \exp(-b_{ij} R_{ij}) \sum_{k=0}^n \frac{(b_{ij} R_{ij})^k}{k!}. \quad (4)$$

The sum over all 49 site-site interactions yields the total interaction potential for a given configuration,

$$V(R, \theta_1, \theta_2, \phi) = \sum_{i=1}^7 \sum_{j=1}^7 V_{ij}[R_{ij}(R, \theta_1, \theta_2, \phi)]. \quad (5)$$

The parameters  $A$ ,  $\alpha$ ,  $b$ ,  $C_6$ , and  $C_8$  for all 28 types of site-site combinations, the site charges  $q$  for all seven sites, and the site positions within the N<sub>2</sub>O monomer were fully optimized in a non-linear least-squares fit to the 2018 calculated interaction energies. We imposed four constraints during the fit.

1. The sum of all site charges had to be zero.
2. The isotropic average of the  $C_6$  dispersion coefficient,  $C_{6\text{ iso}} = \sum_{i=1}^7 \sum_{j=1}^7 C_{6ij}$ , had to be equal to the accurate value of 184.9 a.u.<sup>30</sup> obtained from dipole oscillator strength distributions (DOSDs).
3. The dipole moment had to be  $-0.061\ 080$  a.u.
4. The quadrupole moment had to be  $-2.6710$  a.u.

The multipole moments were obtained from frozen-core CCSD(T)/aug-cc-pV6Z calculations. These values can be

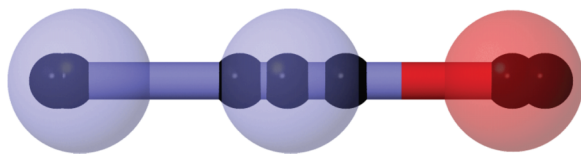


FIG. 1. Visualisation of the optimized positions of the seven interaction sites in the  $\text{N}_2\text{O}$  monomer.

considered converged to within 0.5% of the CBS value. Our multipole results are in very good agreement with those of Chang *et al.*<sup>25</sup> The resulting positions of the interaction sites in the  $\text{N}_2\text{O}$  monomer are visualized in Fig. 1.

Figure 2 shows the high quality of our fit by comparing interaction energies obtained from the potential function with the respective *ab initio* values. We also calculated the mean absolute errors (MAEs) of the fitted PES for three ranges of potential energies. The MAE is 2.05 K for values between the global minimum and +1000 K, 34 K between 1000 K and 5000 K, and 277 K between 5000 K and 30 000 K. In the interval between 30 000 K and the highest energies at about 200 000 K, the MAE increases even more, but this region is practically not relevant for determining thermophysical properties. However, these extreme potential energies were included in the fit to create a physically meaningful and high enough repulsive barrier for safe application of the potential function in computer simulations. During the fit, we also tested reduced sets of input data. For example, we left out a few angular sets or randomly removed up to 25% of all input values to see how well a fit to the remaining points would interpolate the excluded points. As a result of these tests, we have always observed very good interpolation behavior

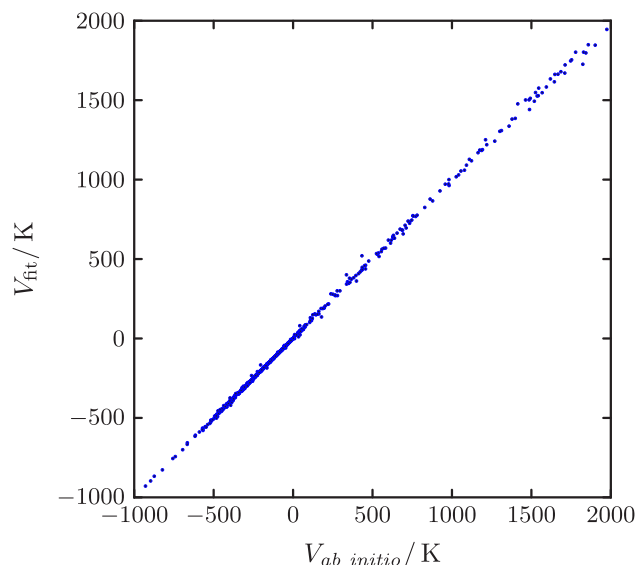


FIG. 2. Interaction energies from the analytical fit as given by Eq. (5) versus *ab initio* calculated interaction energies from Eq. (2).

in support of our chosen sampling-grid density and of the analytical form of the PES in connection with the site-site approach. Furthermore, during the development stages of the fit, we have periodically evaluated the stability of the values of the second virial coefficient. Since the values of the virial coefficient are very sensitive to the shape and depth of the potential, they are a good test criterion to ensure an optimal fit with the minimum necessary number of parameters. Figure 3 illustrates the distance dependence of the fitted analytical potential function and of the *ab initio* values for twelve

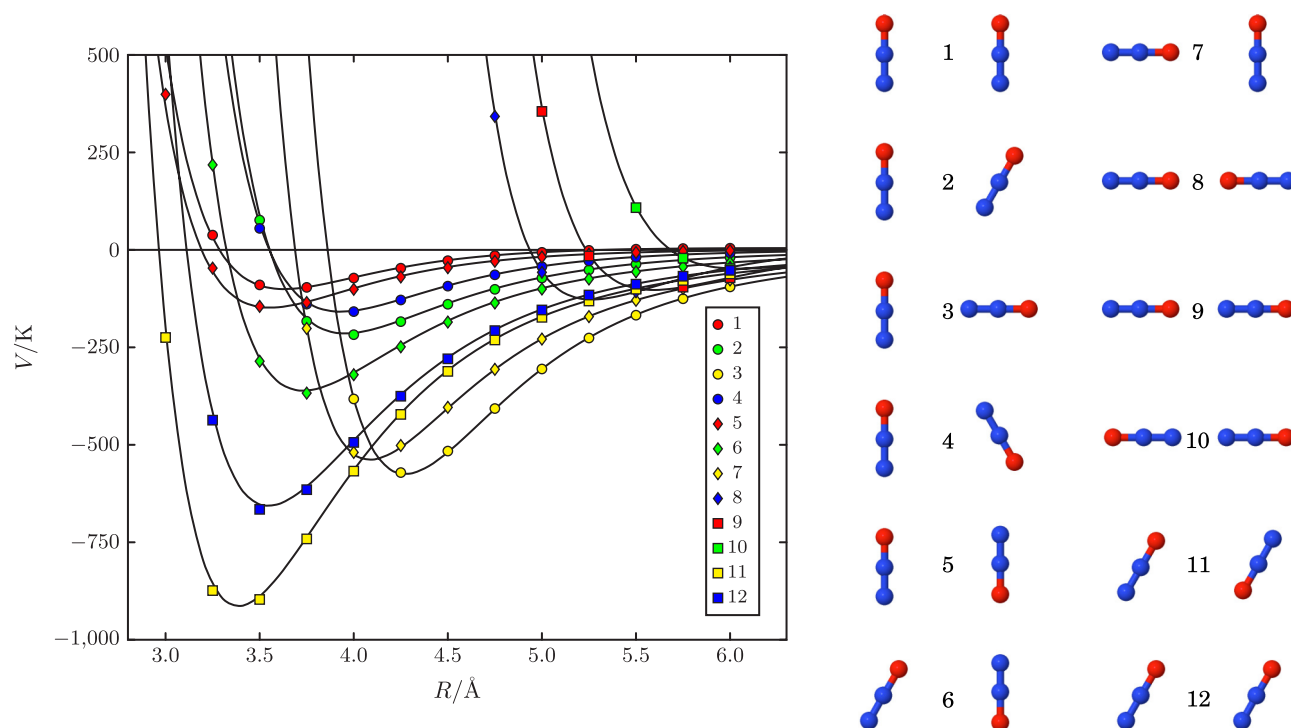


FIG. 3. Distance dependence of the  $\text{N}_2\text{O}$ - $\text{N}_2\text{O}$  interaction potential for 12 selected angular orientations. Configurations 11 and 12 closely resemble the two equilibrium orientations. The *ab initio* calculated values are represented by symbols and the fitted analytical potential function by solid lines.

TABLE I. Comparison of the two minima of the proposed analytical potential function with other recent *ab initio* results.

Pair potential	$R/\text{\AA}$	$\theta_1/\text{deg}$	$\theta_2/\text{deg}$	$\phi/\text{deg}$	$D_e/\text{K}$
Dawes <i>et al.</i> (2010) <sup>a</sup>	3.359	61.17	118.83	180.0	911.4
Zheng <i>et al.</i> (2011) <sup>b</sup>	3.379	60.8	119.2	180.0	902.9
This work	3.359	61.27	118.73	180.0	929.1
Dawes <i>et al.</i> (2010) <sup>a</sup>	3.499	57.77	63.90	0.0	669.3
Zheng <i>et al.</i> (2011) <sup>b</sup>	3.535	56.3	63.9	0.0	669.5
This work	3.516	57.01	64.12	0.0	666.4

<sup>a</sup>Reference 12.<sup>b</sup>Reference 13.

selected angular configurations. We have identified the two minima of our proposed analytical potential function and found good agreement with the *ab initio* results of Refs. 12 and 13, see Table I. The two configurations, a planar slipped parallel one and a planar slipped antiparallel one, closely resemble configurations 11 and 12 in Fig. 3.

The supplementary material<sup>27</sup> contains the parameters of the potential function, a Fortran 90 code for evaluation of the potential, as well as detailed results of the multipole study.

### III. SECOND VIRIAL COEFFICIENT

#### A. Theory

For a gas composed of rigid molecules, the classical second virial coefficient can be written as

$$B_{cl}(T) = -\frac{N_A}{2} \int_0^\infty \langle f_{12} \rangle_{\Omega_1, \Omega_2} d\mathbf{R}, \quad (6)$$

with

$$f_{12} = \exp\left[-\frac{V(\mathbf{R}, \Omega_1, \Omega_2)}{k_B T}\right] - 1. \quad (7)$$

Here,  $\mathbf{R}$  is the distance vector between the centers of mass of the two molecules, and the angular orientations of molecules 1 and 2 are represented by  $\Omega_1$  and  $\Omega_2$ , respectively. The angle brackets denote an average over these angular orientations. Quantum effects have to be considered, especially at low and moderate temperatures. We accounted for this by using the quadratic Feynman-Hibbs effective pair potential<sup>31</sup> for  $V$  in Eq. (7). For the case of two identical rigid linear molecules, the effective potential can be written as<sup>4</sup>

$$V_{QFH}(T) = V + \frac{\hbar^2}{12k_B T} \left[ \frac{1}{m} \left( \frac{\partial^2 V}{\partial x^2} + \frac{\partial^2 V}{\partial y^2} + \frac{\partial^2 V}{\partial z^2} \right) + \frac{1}{2I} \sum_{i=1}^2 \left( \frac{\partial^2 V}{\partial \psi_{a,i}^2} + \frac{\partial^2 V}{\partial \psi_{b,i}^2} \right) \right], \quad (8)$$

where  $m$  is the molecular mass,  $I$  is the moment of inertia, and  $x$ ,  $y$ , and  $z$  are the cartesian components of  $\mathbf{R}$ . The angles  $\psi_{a,i}$  and  $\psi_{b,i}$  correspond to rotations around two arbitrarily chosen principal axes  $a$  and  $b$ , perpendicular to each other, of molecule  $i$ .

### B. Numerical evaluation and results

To determine values for the second virial coefficient, the integral in Eq. (6) is evaluated numerically using the Mayer-sampling Monte Carlo method proposed by Singh and Kofke.<sup>32</sup> This approach involves a biased two-particle importance-sampling Monte Carlo simulation, where the sampling distribution  $\pi$  is chosen to be equal to the absolute value of the integrand  $\tilde{B}$  of the virial coefficient  $B$ , i.e.  $\pi = |\tilde{B}|$ . Trial moves are accepted with a probability of  $\min(1, \pi_{\text{new}}/\pi_{\text{old}})$ . Values for the second virial coefficient are then obtained from the relation

$$B(T) = B_{\text{hs}} \frac{\langle \tilde{B}(T)/\pi \rangle_\pi}{\langle \tilde{B}_{\text{hs}}/\pi \rangle_\pi}, \quad (9)$$

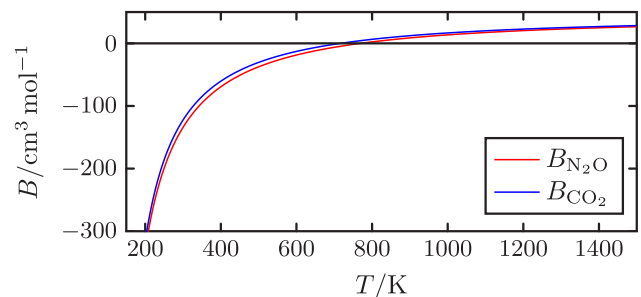
where the hard-sphere fluid serves as the reference system as indicated by the subscript hs. The angle brackets denote the weighted simulation averages. Values for the second virial coefficient were calculated for 77 temperatures between 150 K and 1500 K. All temperatures are considered in a single simulation run<sup>32,33</sup> by calculating the integrand of the virial coefficient for all temperatures at each simulation step, while the sampling distribution is chosen to be the integrand of the virial coefficient at a fixed sampling temperature  $T_s$ . Choosing  $T_s$  to be the lowest temperature of the considered range usually yields the best results. Note that thermal decomposition of real  $\text{N}_2\text{O}$  can occur already well within the considered temperature range at around 800 K.<sup>34</sup> Our final results were obtained by averaging data from 16 independent simulation runs, each one with  $5 \times 10^{10}$  trial moves and  $T_s = 150$  K. The standard uncertainty of the Monte Carlo integration is smaller than  $0.008 \text{ cm}^3 \text{ mol}^{-1}$  for all temperatures.

We fitted the following function to the final values of the second virial coefficient:

$$\frac{B(T)}{\text{cm}^3 \text{ mol}^{-1}} = \sum_{k=-1}^8 a_k (T^*)^{-k} + a_{0.5} \sqrt{T^*} + \frac{a_{-0.5}}{\sqrt{T^*}}, \quad (10)$$

where  $T^* = T/(100 \text{ K})$ . The coefficients in Eq. (10) are  $a_{-1} = 0.2446$ ,  $a_{-0.5} = -5.879$ ,  $a_0 = 79.09$ ,  $a_{0.5} = -37.41$ ,  $a_1 = -318.1$ ,  $a_2 = -564.5$ ,  $a_4 = -1044$ ,  $a_6 = -366.5$ ,  $a_8 = -734.0$ , and  $a_3 = a_5 = a_7 = 0$ . Equation (10) reproduces the calculated values to within  $\pm 0.01 \text{ cm}^3 \text{ mol}^{-1}$ .

We conservatively estimate the total standard uncertainty of our results for  $B(T)$  to be twice the values given by Hellmann<sup>4</sup> for  $\text{CO}_2$ , which were obtained from an *ab initio* PES of the same quality as ours. This is justified by the

FIG. 4. Second virial coefficients of  $\text{N}_2\text{O}$  from Eq. (10) and  $\text{CO}_2$  from Ref. 4.

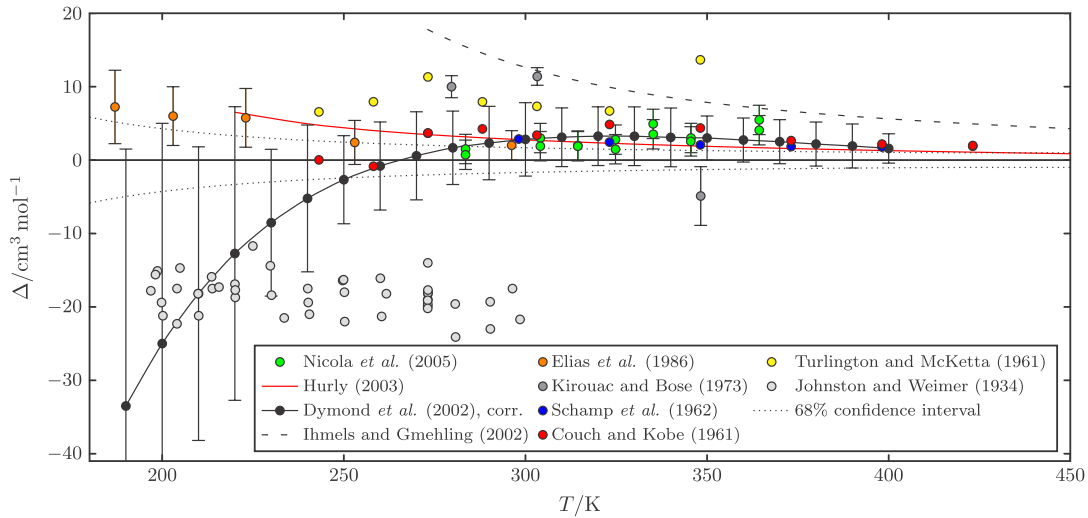


FIG. 5. Absolute deviations,  $\Delta = B_{\text{exp}} - B_{\text{cal}}$ , of experimental data (Refs. 36–44) and of the correlation of Dymond *et al.*<sup>45</sup> for the second virial coefficient of nitrous oxide from values calculated with the *ab initio* PES as a function of temperature. Uncertainties of experimental and correlation data are given as reported by the respective authors.

similar nature of both molecules<sup>35</sup> ( $\text{N}_2\text{O}$  is isoelectronic with  $\text{CO}_2$ ), which results in similar values for  $B(T)$  as can be seen in Fig. 4. The calculated  $B(T)$  data,  $B(T)$  values resulting from Eq. (10), values of the quantum contributions, and the total standard uncertainties are given in the electronic supplementary material.<sup>27</sup>

In Fig. 5, we show the deviations of experimental data<sup>36–44</sup> and of a correlation<sup>45</sup> for the second virial coefficient from our results. The agreement is modest, as most of the values lie outside of our confidence interval. It is obvious that the correlation of Dymond *et al.*<sup>45</sup> is strongly influenced by the data of Johnston and Weimer,<sup>44</sup> who give values that are certainly much too low. Nevertheless, our values are within the 95% confidence limits of the correlation of Dymond *et al.*

## IV. TRANSPORT PROPERTIES

### A. Theory

The kinetic theory of molecular gases<sup>6</sup> is the most suited method for calculating the transport properties in the dilute-gas limit. The shear viscosity  $\eta$  is given by

$$\eta(T) = \frac{k_B T}{\langle v \rangle_0} \frac{f_\eta^{(n)}}{\Xi(2000)}, \quad (11)$$

where  $\langle v \rangle_0 = 4(k_B T / \pi m)^{1/2}$  is the average relative thermal speed,  $\Xi(2000)$  is a temperature-dependent generalized cross section, and  $f_\eta^{(n)}$  is an  $n$ th-order correction factor that accounts for higher basis-function terms in the perturbation-series expansion of the solution of the Boltzmann equation.<sup>6</sup> In the present work, we evaluated  $f_\eta^{(n)}$  up to  $n = 3$ .<sup>4,5</sup>

The thermal conductivity  $\lambda$  has been determined in a second-order approximation. For a pure molecular gas in the rigid-rotor (rr) approximation,  $\lambda$  can be written as

$$\lambda_{\text{rr}}(T) = \frac{5k_B^2 T}{2m \langle v \rangle_0} \left[ \frac{S_{11}^{(1)} - r S_{21}^{(1)}}{S^{(1)}} + \frac{r^2 S_{22}^{(1)} - r S_{12}^{(1)}}{S^{(1)}} \right] f_{\lambda_{\text{rr}}}^{(n)}, \quad (12)$$

with

$$S^{(1)} = \begin{vmatrix} \Xi(1010)_{\text{rr}} & \Xi(1010)_{\text{rr}} \\ \Xi(1001)_{\text{rr}} & \Xi(1001)_{\text{rr}} \end{vmatrix} \quad (13)$$

and

$$r = \left( \frac{2}{5} \frac{C_{\text{rot}}^0}{k_B} \right)^{1/2}, \quad (14)$$

where for linear molecules,  $C_{\text{rot}}^0 = k_B$ . The thermal conductivity of real gases also includes contributions from the transport of vibrational energy, which are neglected in the rigid-rotor approximation. Assuming that the vibrational states of the molecules do not change during collisions and that the influence of the vibrational motion on the trajectories is negligibly small, the vibrational contribution to the thermal conductivity is a simple additive correction,<sup>3,46,47</sup>

$$\lambda = \lambda_{\text{rr}} + \frac{C_{\text{vib}}^0}{m} \mathcal{D}_{\text{self,rr}}, \quad (15)$$

where  $\mathcal{D}_{\text{self,rr}}$  is the product of mass density and self-diffusion coefficient within the rigid-rotor approximation,

$$\mathcal{D}_{\text{self,rr}} = \rho \mathcal{D}_{\text{self,rr}} = \frac{k_B T}{\langle v \rangle_0} \frac{f_{\mathcal{D}_{\text{self,rr}}}^{(n)}}{\sigma'(1000)_{\text{rr}}}. \quad (16)$$

Here,  $\sigma'(1000)_{\text{rr}}$  again denotes a temperature-dependent generalized cross section, see Ref. 3 for details. The expressions for the second-order correction factors  $f_{\lambda_{\text{rr}}}^{(2)}$  and  $f_{\mathcal{D}_{\text{self}}}^{(2)}$  are also given in Ref. 3. We calculated values for  $C_{\text{vib}}^0$  from the vibrational temperatures  $\Theta_1 = 1839.7$  K,  $\Theta_2 = \Theta_3 = 850.8$  K, and  $\Theta_4 = 3149.24$  K, derived by Hurly<sup>37</sup> from accurate speed of sound measurements.

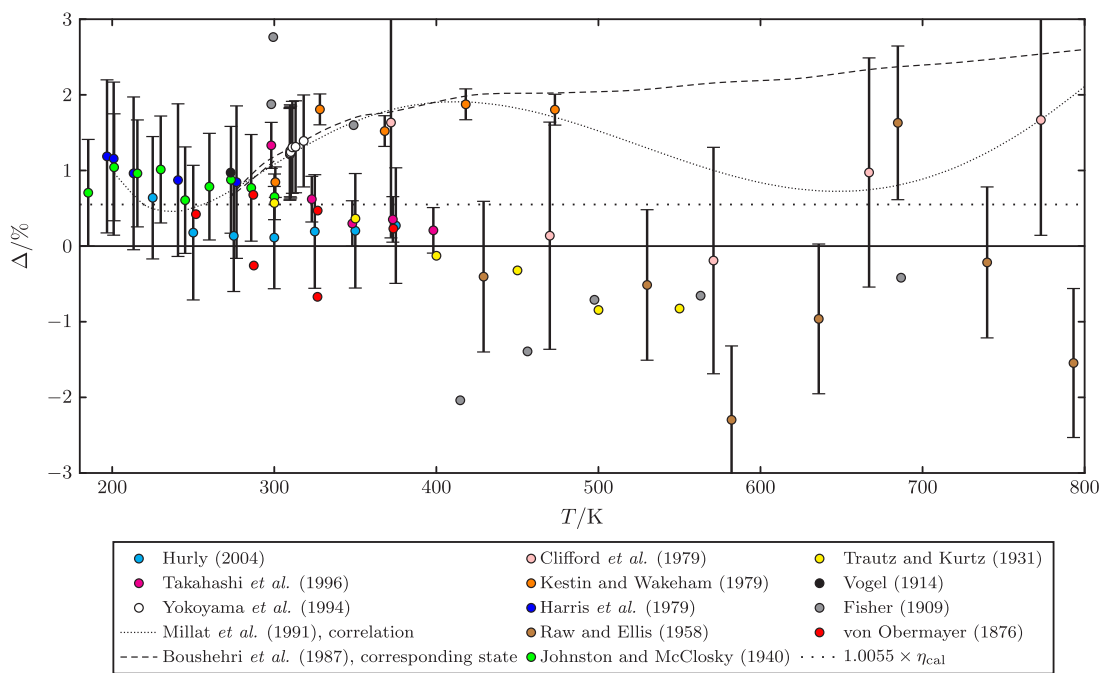


FIG. 6. Relative deviations,  $\Delta = (\eta_{\text{exp}} - \eta_{\text{cal}}) / \eta_{\text{cal}}$ , of experimental data (Refs. 48–60) and of the correlation of Millat *et al.*<sup>61</sup> for the shear viscosity of nitrous oxide in the dilute-gas limit from values calculated with the *ab initio* PES as a function of temperature. Uncertainties of experimental data are given as reported by the respective authors.

## B. Numerical evaluation of the generalized cross sections and results for transport properties

The generalized cross sections needed for the evaluation of the transport properties were computed by means of classical trajectories using a modified version of the *TRAJECT* software code.<sup>7</sup> Classical trajectories describing collisions of two rigid  $\text{N}_2\text{O}$  molecules were obtained by integrating Hamilton's equations from pre- to post-collisional values with an initial and final separation of 500 Å. Choosing such a large separation avoids cutoff effects. Total-energy-dependent generalized cross sections, which are nine-dimensional integrals over the initial states, were calculated for 29 values of a given total energy,  $E = E_{\text{tr}} + E_{\text{rot}}$ , ranging from 60 K to 30 000 K by means of a simple Monte Carlo procedure using quasi-random numbers. Up to  $4 \times 10^6$  trajectories were computed for each total energy value. The number of trajectories had to be reduced for energies below 300 K, because the computational demand required to calculate trajectories with sufficient accuracy increases with decreasing energy. Chebyshev quadrature was used for performing the final integration over total energy to obtain the temperature-dependent generalized cross sections.

The standard uncertainty of the computed transport property values due to the Monte Carlo integration is estimated to be 0.1% for shear viscosity and self-diffusion and 0.2% for thermal conductivity. The calculated values for these three properties in the temperature range of 150 K–1500 K are given in the supplementary material.<sup>27</sup> In his work on  $\text{CO}_2$ , Hellmann<sup>4</sup> recommends a scaling of his values for viscosity by a factor of 1.0055 and for thermal conductivity by a factor of 1.011 based on a comparison with the best available experimental data. The systematic deviations observed for the calculated transport properties are probably caused primarily by the deficiencies of the rigid-rotor approximation. Due to

the similar nature of  $\text{N}_2\text{O}$  and  $\text{CO}_2$ <sup>35</sup> and the fact that we employed the same methodology for obtaining the PES and the transport property values as Hellmann,<sup>4</sup> we recommend the same scaling factors for our  $\text{N}_2\text{O}$  values. We estimate the standard uncertainty of the scaled values for viscosity to be 0.3% between 300 K and 700 K, increasing to 1% at both

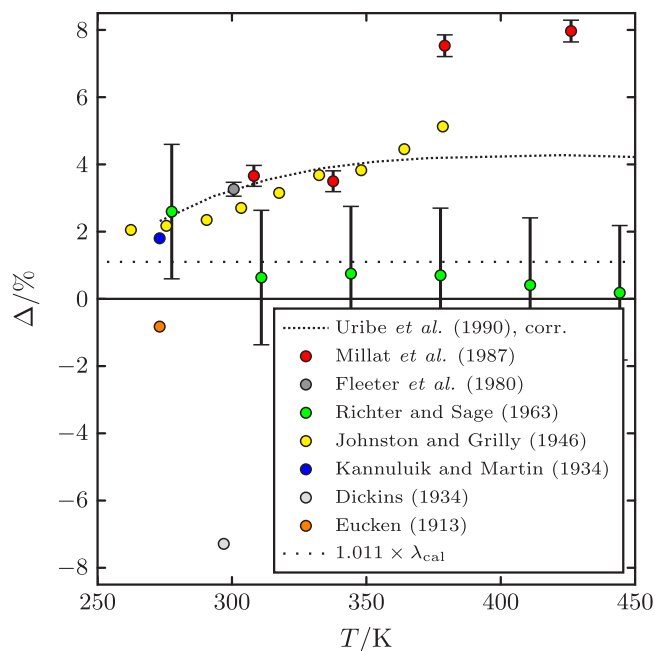


FIG. 7. Relative deviations,  $\Delta = (\lambda_{\text{exp}} - \lambda_{\text{cal}}) / \lambda_{\text{cal}}$ , of experimental data (Refs. 62–68) and of the correlation of Uribe *et al.*<sup>69</sup> for the thermal conductivity of nitrous oxide in the dilute-gas limit from values calculated with the *ab initio* PES as a function of temperature. Experimental uncertainties are given as reported by the respective authors.

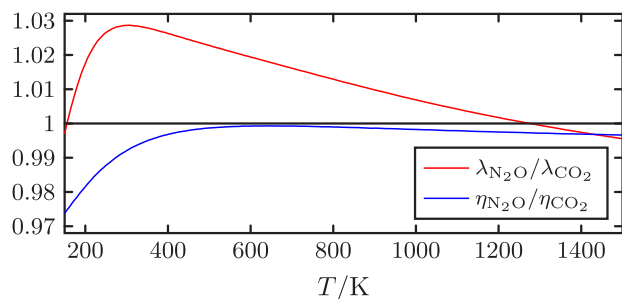


FIG. 8. Ratios of the calculated values for thermal conductivity and shear viscosity of  $\text{N}_2\text{O}$  from the present paper and  $\text{CO}_2$  from Ref. 4.

150 K and 1500 K. For the scaled thermal conductivity values, we estimate the standard uncertainty to be 1% between 300 K and 700 K, increasing to 2% at both 150 K and 1500 K. These are almost the same uncertainty estimates as given by Hellmann.<sup>4</sup> We do not recommend any scaling for the values of the self-diffusion coefficient and estimate their relative standard uncertainty to be 2% for all temperatures.

In Fig. 6, we compare experimental data<sup>48–60</sup> and a correlation<sup>61</sup> for shear viscosity with our values and observe a very good agreement in the temperature trend, especially with the data of Hurly<sup>48</sup> and of Johnston and McClosky.<sup>56</sup> Also the higher temperature values are in general support of our temperature function. The data of Hurly and of Johnston and McClosky are also within an absolute agreement of  $\pm 0.5\%$  with respect to our suggested scaled values. On the other hand, the data of Kestin and Wakeham,<sup>53</sup> which have strongly influenced the correlation of Millat *et al.*,<sup>61</sup> are most probably too large, deviating by about  $+1.5\%$  from the scaled values. It is interesting to note that von Obermayer<sup>60</sup> performed quite accurate measurements for the viscosity of  $\text{N}_2\text{O}$  and other gases as early as 1876.

Figure 7 compares experimental data<sup>62–68</sup> and a correlation<sup>69</sup> with our results on thermal conductivity. We observe good agreement with the datum of Kannuluik and Martin,<sup>66</sup> the datum of Eucken,<sup>68</sup> as well as with most of the data of Richter and Sage.<sup>64</sup> The temperature dependence of the data of Millat *et al.*<sup>62</sup> and of Johnston and Grilly<sup>65</sup> is different from that of our values. Based on our earlier experience with respect to the predictive capabilities of our approach, it is safe to assume that the temperature dependence of our calculated values is the correct one.

There appear to be no experimental data for the self-diffusion coefficient of nitrous oxide in the literature.

Figure 8 shows the ratios of the viscosities of  $\text{N}_2\text{O}$  and  $\text{CO}_2$  and of the thermal conductivities of  $\text{N}_2\text{O}$  and  $\text{CO}_2$ . The values for  $\text{CO}_2$  have been taken from Ref. 4. As expected,<sup>35</sup> the ratios are very close to unity for both properties.

## V. SUMMARY AND CONCLUSIONS

We have determined the first *ab initio* intermolecular PES for two rigid nitrous oxide molecules that is available in analytical form. Interaction energies for 2018 systematically chosen  $\text{N}_2\text{O}-\text{N}_2\text{O}$  configurations were calculated at the CCSD(T) level of theory using the aug-cc-pVTZ and aug-cc-pVQZ basis sets and extrapolated to the CBS limit. The

basis sets were supplemented by a small set of bond functions located midway between the two molecules in all calculations.

An analytical seven-center site-site potential function with isotropic site-site interactions was then fitted to the computed interaction energies as well as to *ab initio* values for the dipole and quadrupole moments, obtained at the frozen-core CCSD(T)/aug-cc-pV6Z level, and to a precise value for the  $C_6$  dispersion coefficient from DOSDs. The PES was used to calculate the second virial coefficient and the dilute-gas transport properties of nitrous oxide in the temperature range from 150 K to 1500 K.

Our values for the second virial coefficient show only modest agreement with the available experimental data, as most of the data lie outside of our confidence interval. On the other hand, the calculated values for shear viscosity are supported by the large body of experimental data. Our viscosity values should be considered for a critical re-evaluation of the correlation of Millat *et al.*<sup>61</sup> The calculated values for thermal conductivity are in good agreement with only a part of the experimental data sets, which enables us to discriminate between contradictory results from different research groups. Based on a recent study on  $\text{CO}_2$ ,<sup>4</sup> a molecule that is isoelectronic with  $\text{N}_2\text{O}$  and has very similar thermophysical property values, we recommend a scaling of our calculated values for viscosity and thermal conductivity by 1.0055 and 1.011, respectively, to obtain values of reference quality.

The computed interaction energies for the 2018 considered  $\text{N}_2\text{O}-\text{N}_2\text{O}$  configurations, the parameters and a Fortran 90 routine of the analytical potential function, as well as all calculated thermophysical property values for dilute nitrous oxide gas are given in the electronic supplementary material.<sup>27</sup>

## ACKNOWLEDGMENTS

This work was financially supported by the Deutsche Forschungsgemeinschaft, Grant Nos. BI 1389/3-1 and BI 1389/3-2.

<sup>1</sup>R. Hellmann, E. Bich, E. Vogel, A. S. Dickinson, and V. Vesovic, *J. Chem. Phys.* **131**, 014303 (2009).

<sup>2</sup>R. Hellmann, E. Bich, E. Vogel, and V. Vesovic, *Phys. Chem. Chem. Phys.* **13**, 13749 (2011).

<sup>3</sup>R. Hellmann and E. Bich, *Mol. Phys.* **113**, 176 (2015).

<sup>4</sup>R. Hellmann, *Chem. Phys. Lett.* **613**, 133 (2014).

<sup>5</sup>J.-P. Crusius, R. Hellmann, E. Hassel, and E. Bich, *J. Chem. Phys.* **141**, 164322 (2014).

<sup>6</sup>F. R. W. McCourt, J. J. M. Beenakker, W. E. Köhler, and I. Kušćer, *Nonequilibrium Phenomena in Polyatomic Gases: Dilute Gases* (Clarendon Press, Oxford, 1990), Vol. 1.

<sup>7</sup>E. L. Heck and A. S. Dickinson, *Comput. Phys. Commun.* **95**, 190 (1996).

<sup>8</sup>Z. S. Huang and R. E. Miller, *J. Chem. Phys.* **89**, 5408 (1988).

<sup>9</sup>N. R. Walker, A. J. Minei, S. E. Novick, and A. C. Legon, *J. Mol. Spectrosc.* **251**, 153 (2008).

<sup>10</sup>H. Valdés and J. A. Sordo, *J. Phys. Chem. A* **108**, 2062 (2004).

<sup>11</sup>G. M. Berner, A. L. L. East, M. Afshari, M. Dehghany, N. Moazzen-Ahmadi, and A. R. W. McKellar, *J. Chem. Phys.* **130**, 164305 (2009).

<sup>12</sup>R. Dawes, X.-G. Wang, A. W. Jasper, and T. Carrington, Jr., *J. Chem. Phys.* **133**, 134304 (2010).

<sup>13</sup>L. Zheng, Y. Lu, S.-Y. Lee, H. Fu, and M. Yang, *J. Chem. Phys.* **134**, 054311 (2011).

<sup>14</sup>T. B. Adler, G. Knizia, and H.-J. Werner, *J. Chem. Phys.* **127**, 221106 (2007).

<sup>15</sup>K. Raghavachari, G. W. Trucks, J. A. Pople, and M. Head-Gordon, *Chem. Phys. Lett.* **157**, 479 (1989).

- <sup>16</sup>K. A. Peterson, T. Adler, and H. J. Werner, *J. Chem. Phys.* **128**, 084102 (2008).
- <sup>17</sup>R. A. Kendall, T. H. Dunning, Jr., and R. J. Harrison, *J. Chem. Phys.* **96**, 6796 (1992).
- <sup>18</sup>S. F. Boys and F. Bernardi, *Mol. Phys.* **19**, 553 (1970).
- <sup>19</sup>C. F. Curtiss, *J. Chem. Phys.* **75**, 1341 (1981).
- <sup>20</sup>E. M. Mas and K. Szalewicz, *J. Chem. Phys.* **104**, 7606 (1996).
- <sup>21</sup>M. Jeziorska, P. Jankowski, K. Szalewicz, and B. Jeziorski, *J. Chem. Phys.* **113**, 2957 (2000).
- <sup>22</sup>R. Bukowski, K. Szalewicz, G. C. Groenenboom, and A. van der Avoird, *J. Chem. Phys.* **128**, 094313 (2008).
- <sup>23</sup>R. Bukowski, K. Szalewicz, G. C. Groenenboom, and A. van der Avoird, *J. Chem. Phys.* **128**, 094314 (2008).
- <sup>24</sup>K. A. Peterson and T. H. Dunning, Jr., *J. Chem. Phys.* **117**, 10548 (2002).
- <sup>25</sup>B. T. Chang, O. Akin-Ojo, R. Bukowski, and K. Szalewicz, *J. Chem. Phys.* **119**, 11654 (2003).
- <sup>26</sup>A. Halkier, T. Helgaker, P. Jørgensen, W. Klopper, H. Koch, J. Olsen, and A. K. Wilson, *Chem. Phys. Lett.* **286**, 243 (1998).
- <sup>27</sup>See supplementary material at <http://dx.doi.org/10.1063/1.4922830> for the parameters, the equilibrium structures, and a Fortran 90 routine of the analytical potential function, details of the multipole moment analysis, results of the *ab initio* calculations for all 2018 points used for the fit of the analytical potential function, and tables of all thermophysical property values calculated in this work.
- <sup>28</sup>CFOUR, Coupled-Cluster techniques for Computational Chemistry, a quantum-chemical program package by J. F. Stanton, J. Gauss, M. E. Harding, and P. G. Szalay with contributions from A. A. Auer, R. J. Bartlett, U. Benedikt, C. Berger, D. E. Bernholdt, Y. J. Bomble, O. Christiansen, M. Heckert, O. Heun, C. Huber, T.-C. Jagau, D. Jonsson, J. Jusélius, K. Klein, W. J. Lauderdale, D. A. Matthews, T. Metzroth, D. P. O'Neill, D. R. Price, E. Prochnow, K. Ruud, F. Schiffmann, S. Stopkowitz, A. Tajti, J. Vázquez, F. Wang, and J. D. Watts and the integral packages MOLECULE (J. Almlöf and P. R. Taylor), PROPS (P. R. Taylor), ABACUS (T. Helgaker, H. J. Aa. Jensen, P. Jørgensen, and J. Olsen), and ECP routines by A. V. Mitin and C. van Wüllen. For the current version, see <http://www.cfour.de>.
- <sup>29</sup>K. T. Tang and J. P. Toennies, *J. Chem. Phys.* **80**, 3726 (1984).
- <sup>30</sup>G. Zeiss and W. J. Meath, *Mol. Phys.* **33**, 1155 (1977).
- <sup>31</sup>R. P. Feynman and A. R. Hibbs, *Quantum Mechanics and Path Integrals* (McGraw-Hill, New York, 1965).
- <sup>32</sup>J. K. Singh and D. A. Kofke, *Phys. Rev. Lett.* **92**, 220601 (2004).
- <sup>33</sup>B. Jäger, R. Hellmann, E. Bich, and E. Vogel, *J. Chem. Phys.* **135**, 084308 (2011).
- <sup>34</sup>E. Hunter, *Proc. R. Soc. A* **144**, 386 (1934).
- <sup>35</sup>A. O. Rankine, *Proc. R. Soc. A* **98**, 369 (1921).
- <sup>36</sup>G. Di Nicola, G. Giuliani, F. Polonara, and R. Stryjek, *Fluid Phase Equilib.* **228–229**, 373 (2005).
- <sup>37</sup>J. J. Hurly, *Int. J. Thermophys.* **24**, 1611 (2003).
- <sup>38</sup>E. C. Ihmels and J. Gmehling, *Int. J. Thermophys.* **23**, 709 (2002).
- <sup>39</sup>E. Elias, N. Hoang, J. Sommer, and B. Schramm, *Ber. Bunsenges. Phys. Chem.* **90**, 342 (1986).
- <sup>40</sup>S. Kirouac and T. Bose, *J. Chem. Phys.* **59**, 3043 (1973).
- <sup>41</sup>H. W. Schamp, Jr., E. A. Mason, and K. Su, *Phys. Fluids* **5**, 769 (1962).
- <sup>42</sup>E. J. Couch and K. A. Kobe, *J. Chem. Eng. Data* **6**, 229 (1961).
- <sup>43</sup>B. L. Turlington and J. J. McKetta, *AIChE J.* **7**, 336 (1961).
- <sup>44</sup>H. L. Johnston and H. R. Weimer, *J. Am. Chem. Soc.* **56**, 625 (1934).
- <sup>45</sup>J. H. Dymond, K. N. Marsh, R. C. Wilhoit, and K. C. Wong, in *Landolt-Börnstein: Numerical Data and Functional Relationships in Science and Technology: New Series, Group IV: Physical Chemistry*, Vol. 21A: Virial Coefficients of Pure Gases, edited by M. Frenkel and K. N. Marsh (Springer, Berlin-Heidelberg-New York, 2002), p. 72.
- <sup>46</sup>Z. Liang and H.-L. Tsai, *Fluid Phase Equilib.* **297**, 40 (2010).
- <sup>47</sup>Z. Liang and H.-L. Tsai, *Mol. Phys.* **108**, 1707 (2010).
- <sup>48</sup>J. J. Hurly, *Int. J. Thermophys.* **25**, 625 (2004).
- <sup>49</sup>M. Takahashi, N. Shibasaki-Kitakawa, C. Yokoyama, and S. Takahashi, *J. Chem. Eng. Data* **41**, 1495 (1996).
- <sup>50</sup>C. Yokoyama, M. Takahashi, and S. Takahashi, *Int. J. Thermophys.* **15**, 603 (1994).
- <sup>51</sup>A. Boushehri, J. Bzowski, J. Kestin, and E. A. Mason, *J. Phys. Chem. Ref. Data* **16**, 445 (1987).
- <sup>52</sup>A. A. Clifford, P. Gray, and A. C. Scott, *J. Chem. Soc., Faraday Trans. 1* **77**, 997 (1981).
- <sup>53</sup>J. Kestin and W. A. Wakeham, *Ber. Bunsenges. Phys. Chem.* **83**, 573 (1979).
- <sup>54</sup>E. J. Harris, G. C. Hope, D. W. Gough, and E. B. Smith, *J. Chem. Soc., Faraday Trans. 1* **75**, 892 (1979).
- <sup>55</sup>C. J. G. Raw and C. P. Ellis, *J. Chem. Phys.* **28**, 1198 (1958).
- <sup>56</sup>H. L. Johnston and K. E. McClosky, *J. Phys. Chem.* **44**, 1038 (1940).
- <sup>57</sup>M. Trautz and F. Kurz, *Ann. Phys.* **9**, 981 (1931).
- <sup>58</sup>H. Vogel, *Ann. Phys.* **43**, 1235 (1914).
- <sup>59</sup>W. J. Fisher, *Phys. Rev.* **28**, 73 (1909).
- <sup>60</sup>A. von Obermayer, *Wien. Ber.* **73**, 433 (1876).
- <sup>61</sup>J. Millat, V. Vesovic, and W. A. Wakeham, *Int. J. Thermophys.* **12**, 265 (1991).
- <sup>62</sup>J. Millat, M. Mustafa, M. Ross, W. A. Wakeham, and M. Zalaf, *Phys. A* **145**, 461 (1987).
- <sup>63</sup>R. Fleeter, J. Kestin, and W. A. Wakeham, *Phys. A* **103**, 521 (1980).
- <sup>64</sup>G. N. Richter and B. H. Sage, *J. Chem. Eng. Data* **8**, 221 (1963).
- <sup>65</sup>H. L. Johnston and E. R. Grilly, *J. Chem. Phys.* **14**, 233 (1946).
- <sup>66</sup>W. G. Kannuluik and L. H. Martin, *Proc. R. Soc. A* **144**, 496 (1934).
- <sup>67</sup>B. G. Dickins, *Proc. R. Soc. A* **143**, 517 (1934).
- <sup>68</sup>A. Eucken, *Phys. Z.* **14**, 324 (1913).
- <sup>69</sup>F. J. Uribe, E. A. Mason, and J. Kestin, *J. Phys. Chem. Ref. Data* **19**, 1123 (1990).